Thiophene-Based Ligands for Histological Multiplex Spectral Detection of Distinct Protein Aggregates in Alzheimer's Disease

Linda Lantz,[a] Hamid Shirani,[a] Bernardino Ghetti,[b] Ruben Vidal,[b] Therése Klingstedt,[a] and K. Peter R. Nilsson*[a]

Abstract: The aggregation and accumulation of proteins in the brain is the defining feature of many devastating neurodegenerative diseases. The development of fluorescent ligands that bind to these accumulations, or deposits, is essential for the characterization of these neuropathological lesions. We report the synthesis of donor-acceptor-donor (D-A-D) thiophene-based ligands with different emission properties. The D-A-D ligands displayed selectivity towards distinct disease-associated protein deposits in histological sections from postmortem brain tissue of individuals affected by Alzheimer's disease (AD). The ability of the ligands to selectively identify AD-associated pathological alterations, such as deposits composed of aggregates of the amyloid-β (Aβ) peptide or tau, was reduced when the chemical composition of the ligands was altered. When combining the D-A-D ligands with conventional thiophene-based ligands, superior spectral separation of distinct protein aggregates in AD tissue sections was obtained. Our findings provide the structural and functional basis for the development of new fluorescent ligands that can distinguish between aggregated proteinaceous species, as well as offer novel strategies for developing multiplex fluorescence detection of protein aggregates in tissue sections.

Introduction

Fluorescent ligands are vital for visualizing accumulations of protein aggregates, which are the pathological hallmarks of many neurodegenerative diseases such as Alzheimer's disease (AD).[1–4] A diversity of molecular scaffolds targeting the cross β-pleated sheet structure of protein aggregates has previously been presented.[5–25] The azo dye Congo Red (CR) was discovered by Bennhold in 1922,[5] and a variety of CR derivatives, including Chrysamine G,[6] X-34,[7] Methoxy-X-04[8] and K114,[9] have been designed to improve the ligands performance for identifying protein deposits. Likewise, a variety of molecular rotors, such as thioflavins and derivatives thereof, have been utilized as ligands for protein aggregates.[10–16] Thioflavin T (ThT)

was introduced as a fluorescent ligand for amyloid detection in 1959 and has since then been the most commonly used ligand for assessing protein fibril formation in vitro.[10–12,14] A derivative of ThT, denoted Pittsburgh compound B (PiB), can also be utilized for positron emission tomography (PET) imaging of Aβ deposits in AD patients.[13] Furthermore, carbazole derivatives and Amino Naphthalenyl-2-Cyano-Acrylate (ANCA)-based ligands have been presented as efficient tools for detection of protein aggregates.[17–20] For the latter, fluorescent differentiation between different types of protein deposits could be afforded due to the stabilization of the ground versus excited states of these ligands as a function of the polarity of their microenvironment.[19,20] A selection of near infrared emissive ligands optimized for optical in vivo imaging of protein aggregates has also been described.[21–26]

Lately, luminescent conjugated oligothiophenes (LCOs) have been used for fluorescence imaging of protein aggregates. Unlike conventional ligands, such as CR and ThT, individual LCOs or combinations of LCOs allow for the spectral assignment of distinct protein deposits in tissue sections.[27–40] From a chemical perspective, several chemical determinants, such as the number of thiophene units and distinct spacing of anionic groups along the thiophene backbone, have been shown to be crucial for achieving superior LCOs for spectral separation of amyloid-β (Aβ) and tau deposits.[28,29,32,33] In addition, a dual staining protocol utilizing a tetrameric LCO and a heptameric LCO was recently used to reveal age-dependent conformational rearrangement within Aβ aggregates in transgenic mice with AD pathology, as well as Aβ polymorphisms in different etiological subtypes of AD.[30,34–36] Overall, LCOs with specific

[a] L. Lantz, Dr. H. Shirani, Dr. T. Klingstedt, Prof. K. P. R. Nilsson
Department of Physics,
Chemistry and Biology
Linköping University
581 83, Linköping, (Sweden)
E-mail: peter.r.nilsson@liu.se

[b] Dr. B. Ghetti, Dr. R. Vidal
Department of Pathology and Laboratory Medicine
Indiana University School of Medicine
Indianapolis, 46202 Indiana (USA)

Chem. Eur. J. **2023**, e202203568 (1 of 12)

© 2023 The Authors. Chemistry - A European Journal published by Wiley-VCH GmbH

Chemistry–A European Journal

Research Article
doi.org/10.1002/chem.202203568

Chemistry
Europe
European Chemical
Societies Publishing

chemical compositions and intrinsic fluorescence qualities can be applied as powerful tools for identifying distinct protein aggregates in tissue sections with several modes of detection, such as full excitation/emission spectra, and fluorescence decay time.[31]

As the fluorescent characteristics of LCOs to some extents are restricted, thiophene-based ligands covering a wider range of emission will be important for designing multiplex detection methodologies for protein aggregates in tissue sections. In this regard, donor-acceptor-donor (D-A-D) thiophene-based ligands were recently presented.[41–43] By replacing the central thiophene moiety with a benzothiadiazole (BTD) unit, pentameric and heptameric ligands, having emission around 700 nm were developed and these D-A-D based ligands showed specific staining of protein aggregates.[41,42] In addition, a heptameric D-A-D based ligand with a distinct spacing of anionic groups

along the backbone could also be utilized for spectral separation of different types of Aβ aggregates in transgenic mice.[43] Thus, D-A-D thiophene-based ligands with different photophysical properties compared to conventional LCOs can be used as additional tools for visualizing disease-associated protein aggregates.

Herein, we present the synthesis and characterization of a set of additional anionic D-A-D based oligothiophene derivatives with different chain length and alternative spacing of carboxylate groups along the backbone (Figure 1). In order to assess distinct chemical determinants that are necessary for optical detection of Aβ and tau deposits, the novel ligands, as well as similar oligothiophenes and previously reported[41,43] D-A-D based oligothiophene derivatives, were applied to human brain tissue sections with AD pathology and their binding towards Aβ and tau aggregates was evaluated. Alterations in
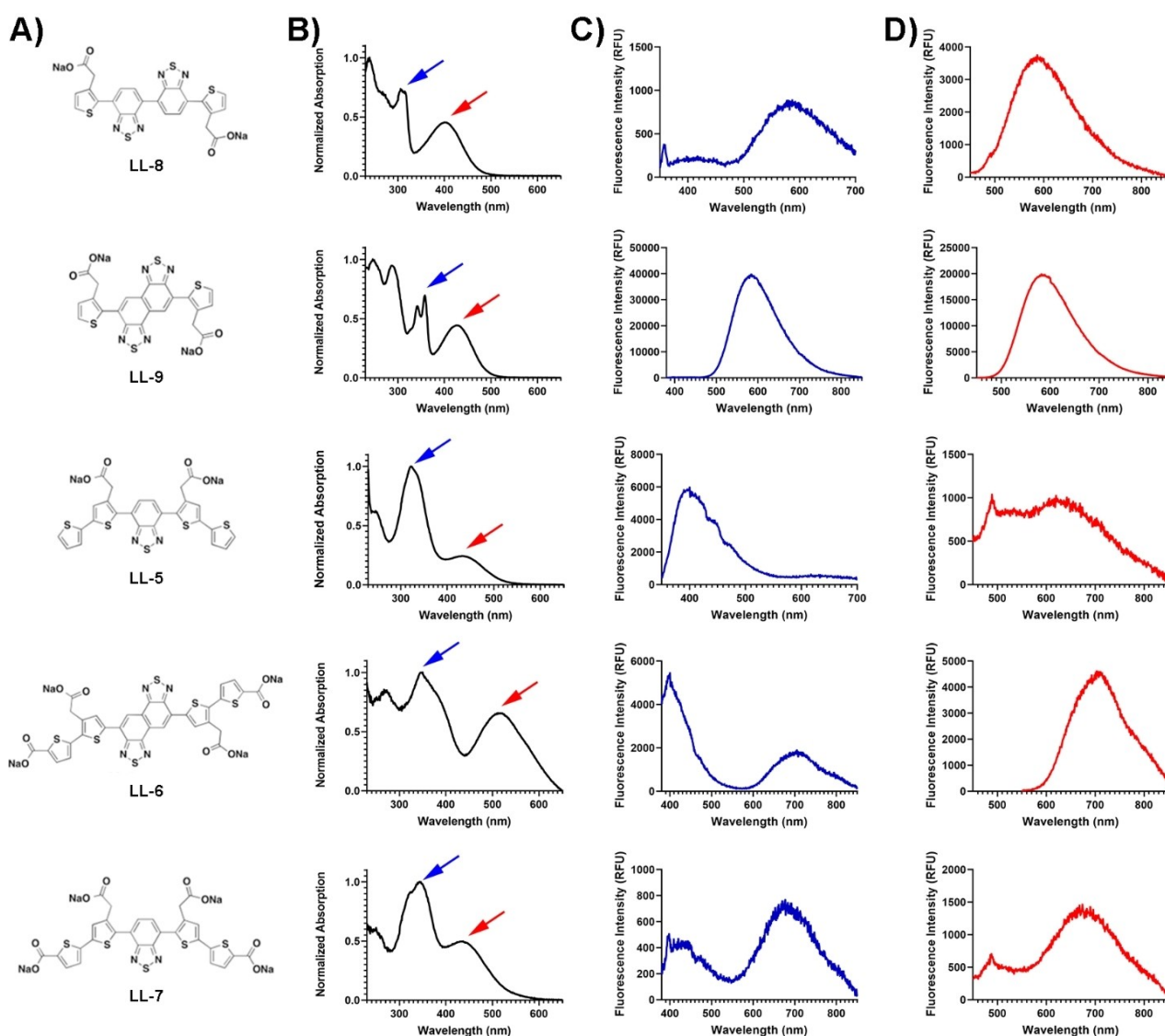
Figure 1. Chemical structure and photophysical properties of the novel D-A-D thiophene-based ligands for protein aggregates. Chemical structure of D-A-D thiophene–based ligands (**A**) and their corresponding absorption- (**B**) and emission spectra (**C–D**). The spectra were recorded for 30 μM ligand in de-ionized water. For the blue emission spectra (**C**), an excitation corresponding to the absorption maximum at shorter wavelengths (blue arrows) was used, whereas an excitation corresponding to the absorption maximum at longer wavelengths (red arrows) was used for the red emission spectra (**D**).

Chem. Eur. J. **2023**, e202203568 (2 of 12)

© 2023 The Authors. Chemistry - A European Journal published by Wiley-VCH GmbH

Chemistry–A European Journal

Research Article
doi.org/10.1002/chem.202203568

Chemistry
Europe
European Chemical
Societies Publishing

the chemical composition of the ligands were shown to reduce or eliminate their capability for identification of Aβ or tau deposits. Thus, these findings might aid in the chemical design of ligands recognizing distinct aggregated proteinaceous species. Finally, a combination of thiophene-based ligands was utilized to design a multiplex detection methodology for superior spectral assignment of different Aβ and tau aggregates in tissue sections.

Results and Discussion

Synthesis and photophysical properties of novel D-A-D thiophene based ligands

In order to generate D-A-D thiophene-based ligands with a chemical diversity, we utilized mono-brominated thiophene building block **1**,[28] a bi-thiophene building block **11**,[32,41] as well as boronic acid pinacol esters of 2,1,3-benzothiadiazole (BTD) **2**, and naphtho[1,2-c:5,6-c']bis([1,2,5]thiadiazole) (NTD) **9**. The thiophene units act as donors and BTD or NTD units as acceptors. By applying palladium-mediated Suzuki-Miyaura cross coupling followed by removal of protecting groups to have anionic side chain functionalities, LL-6, LL-8 and LL-9 were

achieved in affordable yields. In a similar fashion, a di-brominated trimer building block was generated by applying palladium-mediated Suzuki-Miyaura cross coupling followed by N-bromosuccinimide (NBS) in DMF/ chloroform. From this trimer building block, LL-5 and LL-7 were generated by applying symmetric addition of different brominated thiophene building block through Suzuki-Miyaura cross coupling followed by removal of protecting groups to have anionic side chain functionalities (Scheme 1). During the synthesis of compound **3**, a side-product, **8**, was also isolated. This side-product was the homocoupled arylboronic ester, with two BTDs carbon-carbon coupled and a thiophene flanking each side. Palladium catalysed homocoupling of aryl- and heterocyclic boronic acids and boronic esters has been reported to occur under a variety of conditions, though, it is common to occur with oxygen in the system.[44–46] Studies of the influence of electronic effects on homocoupling display that some compounds, for example phenyl boronic acids, bearing electron-donating groups homo-coupled with higher yields than phenyl boronic acids with electron-withdrawing groups.[44] The BTD-BTD homocoupled product was produced as a competing reaction to the Suzuki cross-coupling and appeared in substantial yield under a few tested conditions (solvents), therefore, it can be speculated that one side of the BTD-bispinacol ester was first Suzuki-Miyaura

Scheme 1. Synthesis of different D-A-D thiophene-based ligands. Reagents and conditions: (i) PEPPSI™-IPr, K₂CO₃, 1,4-dioxane/toluene/MeOH (1:1:1), 80 °C, 2 h; (ii) NBS, DMF/chloroform (1:1), −15 °C to r.t., 18 h; (iii) PEPPSI™-IPr, K₂CO₃, toluene/MeOH (1:1), 80 °C, 3 h; (iv) NaOH (1 M, aq.), 1,4-dioxane, 40 °C; (v) PEPPSI™-IPr, Cs₂CO₃, 1,4-dioxane, 80 °C, 3 h; (vi) NaOH, MeOH/CH₂Cl₂ (1:10), r.t., 24 h.

Chemistry–A European Journal

Research Article
doi.org/10.1002/chem.202203568

Chemistry
Europe
European Chemical
Societies Publishing

coupled to a bromothiophene, and due to the thiophene's electron-donating properties, this compound facilitated the homocoupling to another BTD-bispinacol ester on the other side. LL-8 and LL-9 (Figure 1A) resemble the previously synthesized tetrameric oligothiophene t-HTAA[28] (Supporting Information, Figure S1), with a four units long backbone and two carboxylate side chain functionalities at distinct positions, but with a central di-BTD or NTD moiety instead of a bi-thiophene unit. Similarly, LL-5, LL-6 and LL-7 with five units long backbones and two or four carboxylate side chain functionalities at distinct positions resemble the previously reported pentameric LCOs p-HTAA, p-FTAA and HS-84[27,32] (Supporting Information, Figure S1), respectively, but with a central BTD or NTD moiety instead of a thiophene.

When diluted in de-ionized water, all the novel D-A-D ligands displayed distinct absorption- and emission character-istics (Figure 1). Between 300 nm and 600 nm, all ligands showed two absorbance bands (Figure 1B), a high energy band followed by a low energy band, and these bands likely arise from the π-π* transition and the charge-transfer transition, respectively.[41,42] LL-8 displayed a blue-shift of the absorption maxima (310 nm and 410 nm) for both these bands compared to LL-9 (maxima at 350 nm and 425 nm). LL-5, LL-6 and LL-7 showed a similar maximum (around 350 nm) for the high energy band, whereas the lower energy band was more red-shifted for LL-6 (520 nm) compared to LL-5 and LL-7 (440 nm). Upon excitation corresponding to the high energy or low energy absorption band, LL-8 and LL-9 displayed a similar emission with a maximum around 600 nm for both excitation wavelengths (Figure 1C and 1D). In contrast, LL-5 showed a blue-shifted emission spectrum with a maximum around 400 nm when using excitation at the high energy absorption band (Figure 1C), whereas a red-shifted broad emission spectrum (500 nm to 800 nm) with a maximum around 640 nm was obtained with excitation at the lower energy absorption band (Figure 1D). LL-6 and LL-7 demonstrated emission spectra with two distinct emission maxima, 400 nm and 700 nm, when using an excitation related to the high energy absorption band (Figure 1C). A similar emission profile with two distinct emission bands has also been observed for a pentameric D-A-D thiophene based ligand, HS-169, and theoretical calculations have suggested that these emission bands correlate with different electronic transitions.[41,42] Excitation correlated with the high energy absorption band resulted in predominant emission at the longer wavelength (around 700 nm) from both LL-6 and LL-7. Overall, the photo-physical measurements verified that the chemical composition had a great impact on the photo-physical characteristic of the respective ligand.

Histological staining of AD brain tissue sections with D-A-D thiophene-based ligands with different chain lengths

Previous studies of LCOs have shown that the number of thiophene units along the backbone, as well as conformational flexibility of the conjugated backbone, have a major influence on the ligands' ability to detect different protein

aggregates.[28–30,33,47] Therefore, we then examined if similar properties could be observed for D-A-D thiophene-based ligands, and to test this hypothesis, LL-8, LL-9, LL-6, LL-7 and the previously reported heptameric D-A-D thiophene-based ligand LL-1[43] (Supporting Information, Figure S1), were se-lected. In addition, the corresponding tetrameric, pentameric and heptameric LCOs, t-HTAA, p-FTAA, HS-84 and h-FTAA, were included (Supporting Information, Figure S1). To evaluate if the ligands were interacting with Aβ and tau aggregates, 300 nM of ligand was applied for histological staining of human brain tissue sections with AD pathology (Figure 2).

When combined with an antibody towards Aβ (4G8), the tetrameric ligands, LL-8 and LL-9, displayed very weak or no fluorescence from immunopositive cored plaques, diffuse plaques or cerebral amyloid angiopathy (CAA) lesions, whereas the corresponding tetrameric oligothiophene, t-HTAA, showed abundant labelling of cored plaques and CAA, as well as weak fluorescence from diffuse plaques (Figure 2A, Figure S2). Hence, t-HTAA stained strikingly more aggregated Aβ pathology than the tetrameric D-A-D thiophene-based ligands LL-8 and LL-9, suggesting that replacement of the central bi-thiophene moiety with bi-BTD (LL-8) or NTD (LL-9) restricted the ligand detection of aggregated Aβ species. Likewise, the pentameric LCOs, p-FTAA and HS-84, exhibited more pronounced staining of immunopositive cored plaques, diffuse plaques or CAA com-pared to the corresponding pentameric D-A-D thiophene-based ligands, LL-6 and LL-7 (Figure 2B, Figure S3 and S4). Thus, replacing the central thiophene moiety of pentameric LCOs with BTD or NTD resulted in limiting the ligands' ability to detect certain types of Aβ pathology. When bound to cored plaques and CAA, LL-6 and LL-7 displayed blue-shifted emission spectra compared to free ligand in de-ionized water (Support-ing Information, Figure S5), verifying that binding to these Aβ deposits resulted in distinct spectral signatures. The heptameric D-A-D thiophene-based ligand, LL-1, showed similar detection of cored plaques and CAA, as the heptameric LCO h-FTAA (Figure 2C, Figure S6). However, diffuse Aβ plaques displayed more evident staining with h-FTAA than with LL-1, verifying that the substitution of the central thiophene moiety with BTD influenced the detection of certain Aβ deposits also with heptameric thiophene-based ligands. Overall, the D-A-D thiophene-based ligands showed similar results as previously reported for LCOs,[28,47] the pentameric and heptameric D-A-D thiophene-based ligands demonstrated improved detection of Aβ deposits compared to tetrameric D-A-D thiophene-based ligands. In addition, confining the conformational flexibility of the thiophene backbone by replacing central thiophene motifs with BTD, di-BTD or NTD also influenced the performance of the D-A-D thiophene-based ligands, since diffuse plaques were easier to detect with pure oligothiophenes.

When examining the ligands' ability to stain tau pathology, similar trends as for Aβ deposits were seen (Figure 3). For t-HTAA, two of the classical tau pathologies, neurofibrillary tangles (NFTs) and dystrophic neurites could be observed, whereas no tau pathology could be detected with LL-8 or LL-9 (Figure 3A, Figure S7). The pentameric D-A-D thiophene-based ligands LL-6 and LL-7 displayed staining of NFTs and some
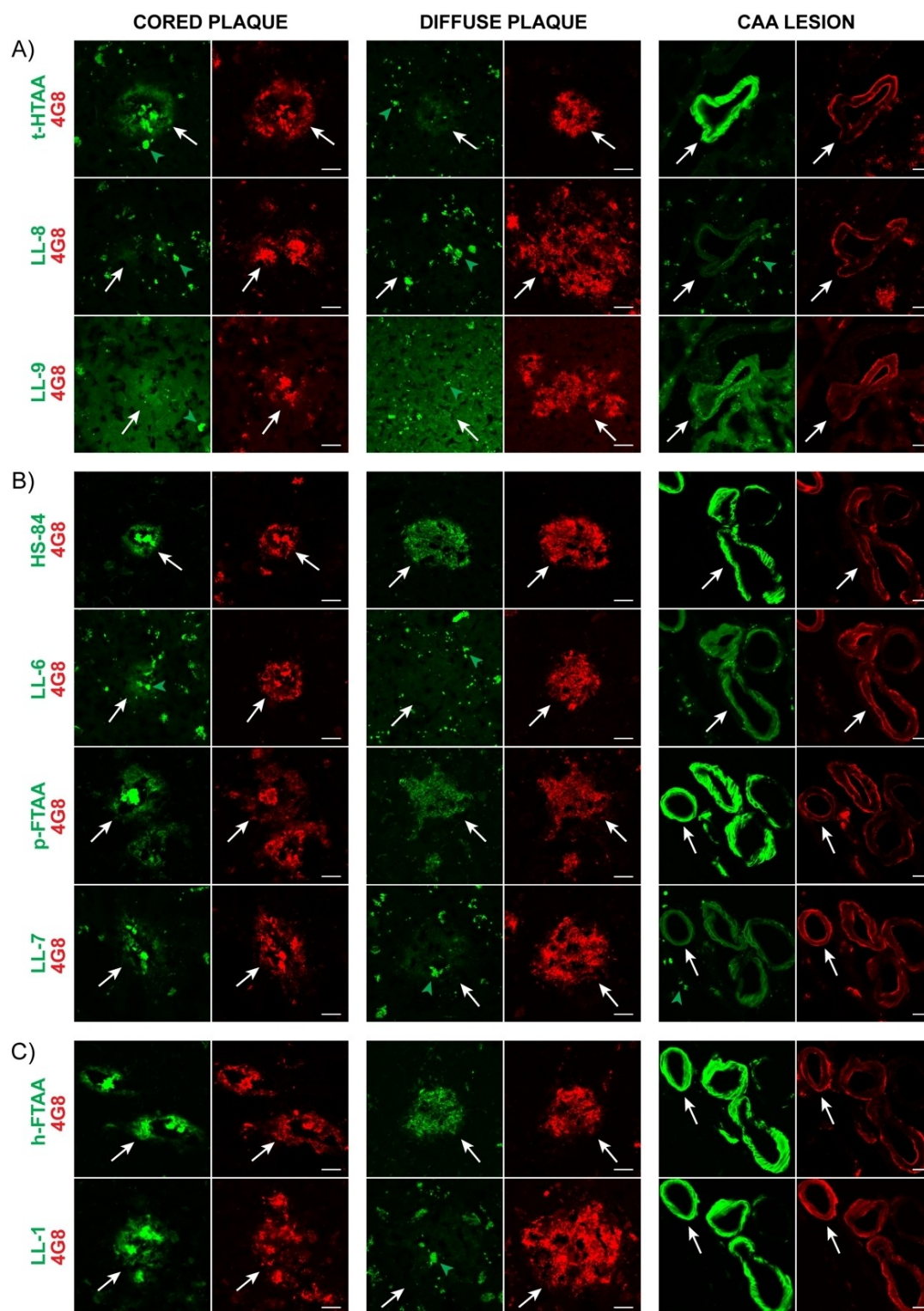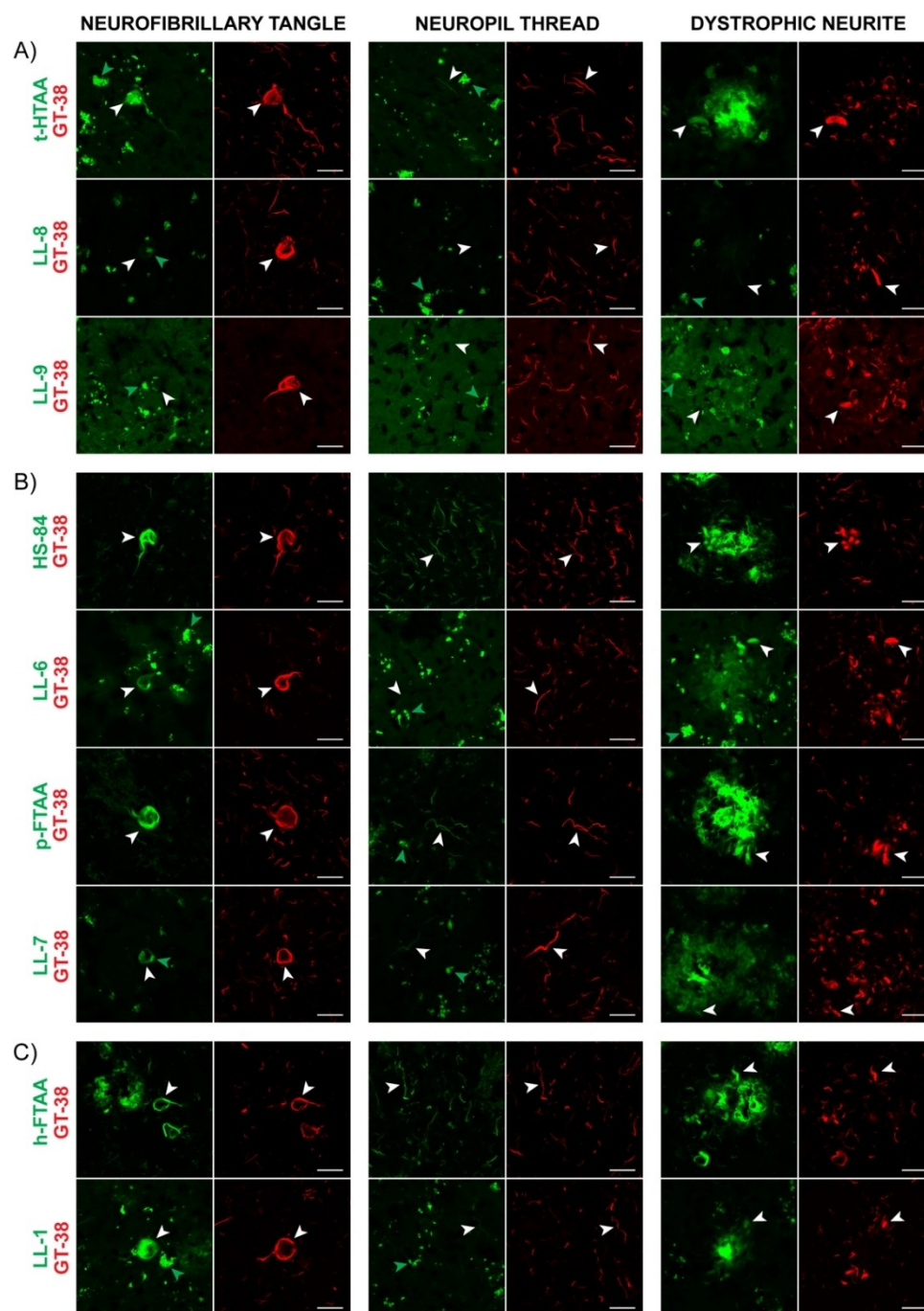
Figure 2. Fluorescence images of brain tissue sections with AD pathology stained with anti-Aβ antibody and different thiophene-based ligands. Images showing staining of different aggregated Aβ pathologies (cored plaques, diffuse plaques and CAA lesion, highlighted by arrows) with anti-Aβ antibody 4G8 (red) and **A)** the tetrameric thiophene-based ligands t-HTAA, LL-8 and LL-9 (green), **B)** the pentameric thiophene-based ligands HS-84, LL-6, p-FTAA and LL-7 (green) or **C)** the heptameric thiophene-based ligands h-FTAA and LL-1 (green). Scale bar represents 20 μm. Autofluorescent lipofuscin granules are highlighted by green arrowheads.

dystrophic neurites (Figure 3B, Figure S8 and S9). However, these two lesions, as well as neuropil threads, could be observed with HS-84 and p-FTAA, the pentameric LCOs (Figure 3B, Figure S8 and S9). Hence, similar to the results obtained

Figure 3. Fluorescence images of brain tissue sections with AD pathology stained with anti-tau antibody and different thiophene-based ligands. Images showing staining of different aggregated tau pathologies (neurofibrillary tangles, neuropil threads and dystrophic neurites, highlighted by white arrowheads) with anti-tau antibody GT-38 (red) and **A)** the tetrameric thiophene-based ligands t-HTAA, LL-8 and LL-9 (green), **B)** the pentameric thiophene-based ligands HS-84, LL-6, p-FTAA and LL-7 (green) or **C)** the heptameric thiophene-based ligands h-FTAA and LL-1 (green). Scale bar represents 20 μm. Autofluorescent lipofuscin granules are highlighted by green arrowheads.

for Aβ pathology, the pentameric LCOs stained a wider selection of tau deposits compared to pentameric D-A-D thiophene-based ligands. All three types of tau lesions could be observed with the heptameric ligands h-FTAA and LL-1 (Figure 3C, Figure S10). Thus, like the observations for aggregated Aβ deposits, the pentameric and heptameric D-A-D thiophene-

based ligands demonstrated improved detection of tau deposits compared to tetrameric D-A-D thiophene-based ligands.

Histological staining of AD brain tissue sections with pentameric and heptameric D-A-D thiophene-based ligands with distinct spacing of anionic groups along the backbone

Distinct spacing and amount of anionic groups along the thiophene backbone are other chemical determinants that have been shown to be crucial for distinguishing protein aggregates with LCOs.[33] To test if a similar performance could be observed for D-A-D thiophene-based ligands, we tested two additional pentameric ligands, LL-5 (Figure 1A) and HS-169 (Supporting Information, Figure S1),[41] with different spacing and amount of anionic groups along the conjugated backbone compared to LL-6 and LL-7 (Figure 1A). As described above, 300 nM of ligand was applied for histological staining of human brain tissue sections with AD pathology. For both HS-169 and LL-5, cored plaques, diffuse plaques and CAA lesions could readily be observed (Figure 4). In addition, tau pathology, such as NFTs, neuropil threads and dystrophic neurites displayed bright fluorescence with both HS-169 and LL-5 (Figure 4, Figure S11). Thus, diffuse Aβ plaques and tau neuropil threads that were not stained by the pentameric D-A-D thiophene-based ligands, LL-6 and LL-7 (Figures 2B and 3B), could be visualized by HS-169 and LL-5. Previous studies[48–50] have shown that anionic LCOs, in a

similar fashion as Congo Red,[51] interact with regularly spaced cationic lysine residues positioned in well-accessible grooves on the fibril surface, and that the spacing of the carboxylic groups along the oligothiophene backbone influences the affinity of the LCO towards the protein aggregate. In addition, the amount of carboxylic acid side chain functionalities, as well as their spacing along the conjugated backbone, were recently assigned as crucial chemical determinants for achieving heptameric D-A-D thiophene-based ligands superior for spectral separation of aggregated Aβ species in brain tissue from transgenic mice.[43] Similar to LL-7, HS-169 has four carboxylate side chain functionalities, but the positions of the acetate side chains are altered on the thiophene rings adjacent to the central BTD moiety. Thus, HS-169 is an isomer to LL-7, having the acetate side chains of the central trimeric thiophene-BTD-thiophene unit tail-to-tail instead of head-to-head. LL-6 also has a similar chemical configuration as HS-169, but replacement of the BTD moiety with an NTD motif shifts the distance between the acetate side chains of the central trimeric building block. LL-5 has a similar configuration as LL-7 with the acetate side chains of the central trimeric thiophene-BTD-thiophene unit positioned head-to-head; however, the LL-5 structure only contains two carboxylate side-chain functionalities since the α-terminal
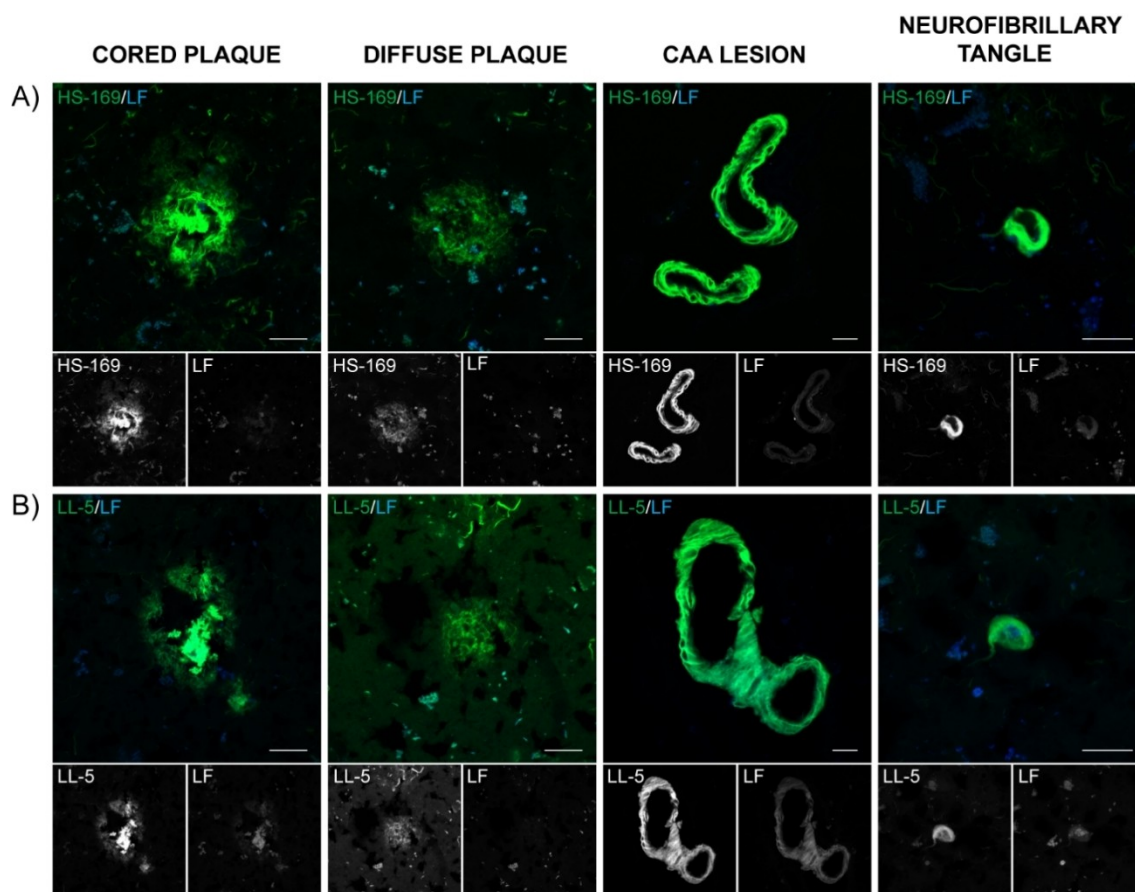

Figure 4. Fluorescence images of brain tissue sections with AD pathology stained with the pentameric D-A-D thiophene-based ligands HS-169 or LL-5. Images showing staining of different aggregated Aβ species (cored plaques, diffuse plaques and CAA lesions) and tau pathology (neurofibrillary tangles) with **A)** HS-169 (green) or **B)** LL-5 (green). Autofluorescence from lipofuscin can be seen in blue. Single channels are shown in white to enhance visualization. Due to some spectral overlap, ligand fluorescence can occasionally also be observed in the lipofuscin channel. Scale bar represents 20 μm.

Chemistry–A European Journal

Research Article
doi.org/10.1002/chem.202203568

Chemistry
Europe

European Chemical
Societies Publishing

carboxylic groups are lacking. Thus, minor re-arrangements of the carboxylic groups, as well as the number of anionic charges, along the conjugated backbone influenced the binding of pentameric D-A-D thiophene-based ligands to both Aβ and tau pathology in human AD brain tissue sections.

Histological staining of AD brain tissue sections with a combination of thiophene-based ligands

Previous studies have shown that a combination of LCOs can be utilized for spectral assignment of different Aβ and tau aggregates in tissue sections.[30,34–36] However, the ligands used in the dual staining protocols show rather large spectral overlap, which might limit the spectral assignment of distinct proteinaceous species. In this regard, combinations of LCOs and D-A-D thiophene-based ligands might offer a better spectral resolution, since these classes of ligands display completely different emission properties. In addition, as shown above, D-A-D thiophene-based ligands and their corresponding oligothiophene derivative detect different types of protein aggregates. Based on our previous findings, as outlined above, we tested a dual staining protocol with 300 nM t-HTAA (Supporting Information, Figure S1) and 300 nM HS-169 (Figure S1). Since t-HTAA and HS-169 show completely different excitation- and emission characteristics,[28,41] the stained AD brain tissue section

was analyzed with a two-channel mode setup reflecting these photophysical parameters. For t-HTAA, excitation at 405 nm and detection of emission between 470 nm to 545 nm were used, whereas excitation at 550 nm and detection of emission between 610 nm to 745 nm were applied for HS-169. When examining an overview of the brain tissue section, distinct areas with differential staining patterns of t-HTAA (green color) and HS-169 (red color) were observed (Supporting Information, Figure S12). Vascular Aβ deposits, CAA, displayed rather homogenous staining patterns with both t-HTAA and HS-169 (Figure 5A). The presence of both ligands on these aggregated Aβ species was also verified by fluorescence lifetime imaging (FLIM). When using 405 nm as excitation wavelength, a distribution of decays (200 ps to 600 ps) corresponding to t-HTAA was observed, whereas excitation at 550 nm rendered a distribution of longer decay times (3500 ps to 5500 ps), similar to those previously reported for HS-169 (Figure 5A).[42] Thus, both these ligands stained vascular Aβ deposits. In contrast, diffuse Aβ plaques were only labelled by HS-169, since they could only be observed in the red channel with the photophysical settings used for HS-169 (Figure 5B). In the green channel, used for t-HTAA emission, only autofluorescent lipofuscin granules surrounding the Aβ aggregates were observed. These observations were also confirmed by FLIM. With excitation at 550 nm, longer decay times, corresponding to HS-169, were displayed from the diffuse Aβ deposits, whereas no
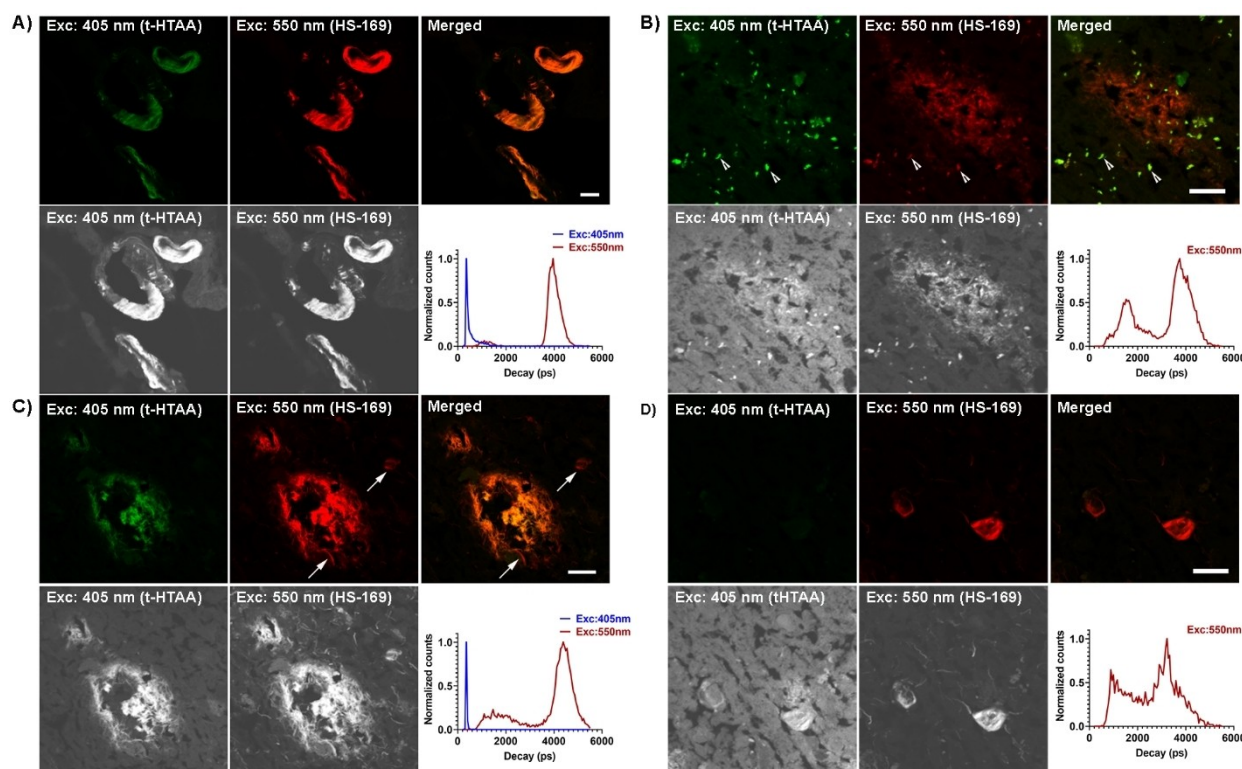

Figure 5. Fluorescence assignment of protein aggregates in brain tissue sections with AD pathology stained with t-HTAA and HS-169. Color-coded fluorescence images (top panel), FLIM intensity images and fluorescence decays (bottom panel) of **A)** CAA lesions, **B)** diffuse Aβ plaques, **C)** neuritic Aβ plaques and **D)** NFTs, stained with t-HTAA and HS-169. For t-HTAA, an excitation at 405 nm was used and emission was recorded between 470 nm to 545 nm, whereas HS-169 was excited at 550 nm and detection of emission between 610 nm to 745 nm was applied. Autofluorescence from lipofuscin in (**B**) are highlighted with white arrow heads, whereas HS-169 stained tau pathology in (**C**) is shown with white arrows. Scale bars represent 20 μm.

Chemistry–A European Journal

Research Article
doi.org/10.1002/chem.202203568

Chemistry Europe
European Chemical
Societies Publishing

adequate decay times could be obtained when using the FLIM settings (excitation at 405 nm) for t-HTAA (Figure 5B). With excitation at 550 nm, decays times (600 ps to 3000 ps) from the autofluorescent lipofuscin structures were also detected.

When analysing the emission profiles from neuritic plaques, fluorescence from both ligands could be detected, and also FLIM revealed distribution of decays correlating to both t-HTAA and HS-169 (Figure 5C). However, dystrophic neurites infiltrating the plaques and neuropil threads surrounding the Aβ pathology only displayed HS-169 emission characteristics and a distribution of decays related to this ligand (Figure 5C). Similar results were observed for NFTs (Figure 5C). Hence, aggregated tau was only stained by HS-169, whereas different types of Aβ pathology displayed a variation in t-HTAA and HS-169 staining patterns.

To test an additional combination of an LCO and a D-A-D thiophene-based ligand for multiplex spectral detection of distinct protein aggregates in human AD tissue section, we next utilized a dual staining protocol with the two pentameric ligands p-FTAA (Supporting Information, Figure S1) and LL-5 (Figure 1). In contrast to the previous combination of ligands, t-HTAA and HS-169, the same excitation wavelength, 490 nm, can be used for p-FTAA and LL-5, allowing simultaneous spectral imaging and FLIM. Like the previous dual staining protocol, areas with different ligand staining patterns were observed when assessing an overview of the brain tissue section (Figures 6A–D). CAA and neuritic plaques displayed spectral profiles with the characteristic emission spectra for both p-FTAA (emission maxima at 515 nm and 545 nm)[27] and LL-5 (emission maximum at 625 nm) (Figure 6E). However, the emission from
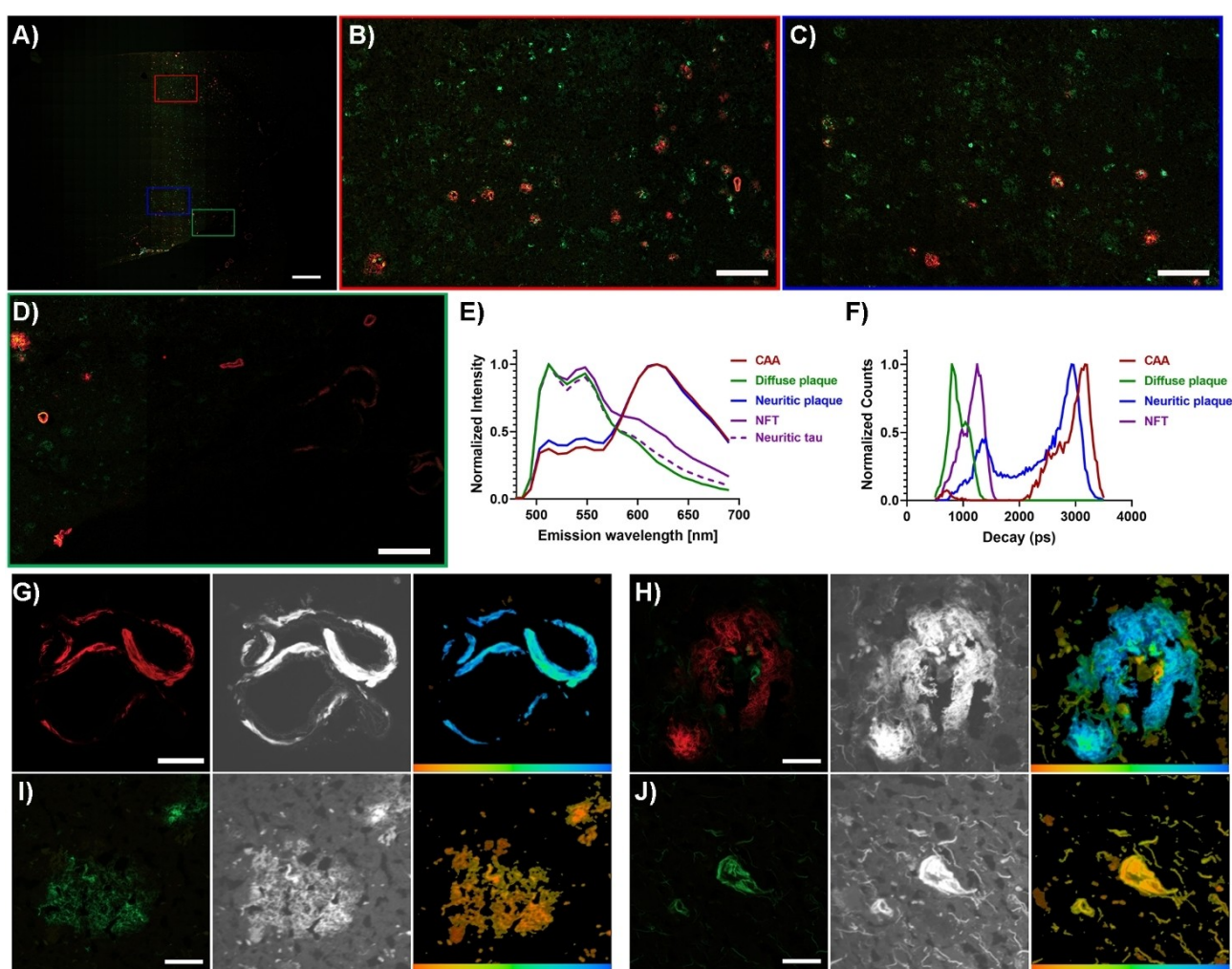

Figure 6. Fluorescence assignment of protein aggregates in brain tissue sections with AD pathology stained with p-FTAA and LL-5. **A)** Overview image of the whole tissue section showing the correlation between p-FTAA (green) and LL-5 (red) staining. **B–D)** Zoom in of the different regions highlighted in (**A**). Red square (**B**), blue square (**C**) and green square (**D**). **E)** Emission spectra from different aggregated Aβ (CAA, diffuse and neuritic plaque) and tau (NFTs and dystrophic neurites) with excitation at 490 nm. The p-FTAA emission maxima are observed at 515 nm and 545 nm, whereas LL-5 displays an emission maximum at 625 nm. **F)** Fluorescent decays from different aggregated Aβ pathologies (CAA, diffuse and neuritic plaque) and tau pathologies (NFTs and dystrophic neurites) with excitation at 490 nm. The distribution of decays for p-FTAA is observed between 600 ps to 1200 ps, whereas LL-5 displays distributions of decays between 2000 ps to 3500 ps. **G–J)** Spectral images (left panel), FLIM images (middle panel) and color-coded FLIM images (right panel) from different aggregated Aβ pathologies, CAA (**G**), neuritic (**H**) and diffuse plaque (**I**)) and tau pathologies, NFTs (**J**) with excitation at 490 nm. The color bars (right panel) represent 500 ps to 3500 ps. Scale bars represent 1000 μm (A), 200 μm (**B–D**), 50 μm (**G**) and 20 μm (**H–J**).

Chemistry–A European Journal

Research Article
doi.org/10.1002/chem.202203568

Chemistry Europe
European Chemical
Societies Publishing

LL-5 was more pronounced than the fluorescence from p-FTAA, and when analysed with FLIM, these aggregated Aβ pathologies predominantly displayed distributions of decays (2000 ps to 3500 ps) related to LL-5 (Figures 6F–H). As reported previously,[31] p-FTAA bound to protein aggregates displays shorter decays, 600 ps to 1200 ps, and such decays were observed from diffuse Aβ aggregates (Figures 6F and 6I) and aggregated tau pathology, such as NFTs and tau deposits infiltrating or surrounding the neuritic plaques, whereas the distribution of decays (2000 ps to 3000 ps) related to LL-5 was completely lacking (Figures 6F, 6H and 6 J). Thus, in contrast to CAA and neuritic plaques, diffuse Aβ deposits, as well as tau lesions, were only stained by p-FTAA. The observations from FLIM were also verified by spectral analysis since these aggregated species displayed an emission profile related to p-FTAA (Figure 6E). Notably, as reported previously,[27,28] p-FTAA displayed a slightly red-shifted emission profile when bound to tau aggregates compared to Aβ deposits (Figure 6E). This aggregate specific photophysical alteration could also be observed with FLIM, which showed that tau deposits stained with p-FTAA displayed slightly longer decay times compared to p-FTAA labelled Aβ deposits (Figure 6F).

In general, the observations from the dual staining set ups agree with the results obtained when using the single ligands. t-HTAA only displayed weak staining towards diffuse Aβ plaques and NFTs, whereas HS-169 clearly labelled both types of deposits. Hence, only HS-169 was observed from these aggregated pathologies when using the combination of ligands. For the second protocol, dual staining with p-FTAA and LL-5, the difference in staining patterns of the ligands is most likely due to a competition between the ligands towards different aggregates, since both ligands stained all the aggregated pathologies when used individually. Hence, LL-5 most likely have a better affinity for CAA and neuritic Aβ deposits, whereas p-FTAA binds better to diffuse Aβ plaques and NFTs. From a chemical perspective, the preferential binding towards certain protein aggregates might be associated with the overall net charge of the pentameric ligand. p-FTAA has four anionic groups, whereas LL-5 only has two carboxylate groups, suggesting that four anionic groups are necessary for achieving a more optimal interaction with diffuse Aβ deposits and tau pathologies. Likewise, less charges along the conjugated backbone seems to favour binding towards CAA and neuritic Aβ deposits. From a biochemical perspective, the length of the accumulated Aβ peptides is different in parenchymal deposits compared to vascular Aβ deposits.[52–54] In addition, cored plaques and CAA show intense staining with conventional amyloid ligands, such as Thioflavin T and Congo red, whereas diffuse plaques are only faintly labelled with these agents.[55] Likewise, a tetrameric and a heptameric LCO displayed alternative binding to Aβ deposits comprised of specific variants of Aβ 1-40 or Aβ 1-42.[36] Hence, the difference in binding of the ligands used for the dual staining protocols might be due to chemical variations of the ligands, as well as various biochemical composition of the protein aggregates.

Overall, the dual staining experiments showed that the combination of a pure oligothiophene and a D-A-D thiophene-based ligands can be utilized to assign different aggregated Aβ and tau pathologies in human AD brain tissue sections. Previous studies have shown that combinations of small fluorescent ligands,[56,57] as well as different oligothiophenes,[30,34–36,58] can efficiently be employed to reveal different aggregated Aβ deposits in transgenic mice with Aβ pathology, or Aβ polymorphisms in different etiological subtypes of AD. Hence, it would be interesting to apply the dual staining protocols reported herein towards brain sections from transgenic mice with distinct Aβ deposits, as well as comparing different classes of AD, such as sporadic, familiar and rapidly progressive AD. In addition, staining protocols with different combination of ligands might also be of relevance for protein aggregates in other proteopathic neurodegenerative diseases, since a structural polymorphism has also been reported for tauopathies.[59–63]

Conclusions

In conclusion, we have developed a new set of D-A-D thiophene-based ligands that selectively target Aβ and tau deposits in AD brain tissue sections. Similar to pure oligothiophenes, the selectivity of a distinct ligand was highly dependent on several chemical determinants, such as the length and flexibility of the conjugated backbone, as well as the amount and spacing of anionic groups along the conjugated backbone. In addition, dual staining protocols with different combinations of an oligothiophene and a D-A-D thiophene-based ligands allowed multiplex spectral detection of distinct protein aggregates in tissue sections with AD pathology. Our findings provide useful knowledge of how minor changes of the chemical structure of D-A-D thiophene-based ligands influence their binding properties towards different protein aggregtes, as well as expand the toolbox of fluorescent ligands that can be utilized for fluorescent assignment of distinct aggregated proteinaceous species. We foresee that dual staining protocols with thiophene-based ligands will aid in studying the pathological relevance of distinct protein deposits in several protein aggregation diseases.

Experimental Section

Full experimental details including additional characterization data and NMR spectra of new compounds, as well as supporting figures and tables are given in the Supporting Information.

Synthesis of ligands: The synthesis of t-HTAA, p-FTAA, HS-84, h-FTAA, LL-1 and HS-169 has been published elsewhere.[27,28,32,41,43] The detailed synthesis of the other precursor molecules and ligands is described in the Supporting Information.

Optical characterization of the ligands: Stock solutions of ligands (1.5 mM in de-ionized water) were diluted to 30 μM in de-ionized water. Excitation- and emission spectra of the ligands were collected using an Infinite M1000 Pro microplate reader (Tecan, Männedorf, Switzerland).

Ligand and antibody double staining: Frozen brain tissue from a neuropathologically confirmed case of Alzheimer's disease (AD) was obtained from the Dementia Laboratory at the Department of

Chemistry–A European Journal

Research Article
doi.org/10.1002/chem.202203568

Chemistry Europe
European Chemical
Societies Publishing

Pathology and Laboratory Medicine, Indiana University School of Medicine, Indianapolis, USA.
The studies carried out at the Indiana University School of Medicine were reviewed by the Indiana University Institutional Review Board. An autopsy consent including permission to carry out research on tissue obtained *post mortem* was obtained from the legal next of kin at the time of the affected individual's death. The experiments performed at Linköping University were reviewed and approved by a national ethical committee (approval number 2020–01197). Sections of frontal cortex (10 μm) were fixed in 70% EtOH for 3 min at 4°C, incubated 2×2 min in dH2O at RT and then 10 min in phosphate buffered saline (PBS, 10 mM phosphate, 140 mM NaCl, 2.7 mM KCl, pH 7.4). After a blocking and permeabilization step in PBS with 0.1% triton x-100 (PBS-T) and 5% normal goat serum for 1 h, the primary antibody, mouse monoclonal 4G8 (Biolegend) or mouse monoclonal GT-38 (Abcam), reactive against the amyloid-β peptide or AD tau, respectively, was added. Both antibodies were diluted 1:1000 in PBS-T containing 5% normal goat serum, and the length of incubation was 16 h at 4°C. The sections were washed in PBS-T and then incubated with goat anti-mouse secondary antibodies conjugated with Alexa 488, 594 or 647 (ThermoFisher) diluted 1:400 in PBS-T containing 5% normal goat serum for 1 h at RT. After washing in PBS, the sections were incubated with 300 nM LL-1, LL-6, LL-7, LL-8, LL-9, t-HTAA, p-FTAA, HS-84 or h-FTAA in PBS for 30 min at RT. The sections were then washed with PBS three times and mounted with Dako mounting medium for fluorescence (Agilent). The mounting medium was allowed to solidify at least overnight before sealing the cover slips with nail polish. The result was analysed using an inverted Zeiss LSM 780 laser scanning confocal microscope (Zeiss) using the following excitation/emission settings: LL-1: ligand 550/555-680 nm; antibody 490/499-632 nm; lipofuscin 405/410-514 nm, LL-6: ligand 550/555-680 nm; antibody 490/499-632 nm; lipofuscin 405/410-514 nm, LL-7: ligand 550/555-696 nm; antibody 490/499-579 nm; lipofuscin 405/410-499 nm, LL-8: ligand 405/565-708 nm; antibody 490/499-597 nm; lipofuscin 568/585-712 nm, LL-9: ligand 405/565-711 nm; antibody 490/499-597 nm; lipofuscin 568/585-712 nm, t-HTAA: ligand 405/410-514 nm; antibody 633/638-755 nm; lipofuscin 561/570-632 nm, p-FTAA: ligand 458/484-706 nm; antibody 633/647-755 nm; lipofuscin 580/588-632 nm, HS-84: ligand 458/484-706 nm; antibody 633/647-755 nm; lipofuscin 580/588-641 nm, h-FTAA: ligand 490/499-632 nm; antibody 633/638-755 nm; lipofuscin 405/410-514 nm.

Ligand staining: Sections of frontal cortex (10 μm) from an AD patient were fixed in 96% EtOH for 10 min at RT, incubated 10 min in 50% EtOH followed by 10 min in dH2O at RT and then 10 min in PBS. The sections were incubated with 300 nM of the respective ligand in PBS for 30 min at RT. The sections were then washed with PBS three times and mounted with Dako mounting medium for fluorescence (Agilent). The mounting medium was allowed to solidify at least overnight before sealing the cover slips with nail polish. The sections were analysed using an inverted Zeiss LSM 780 laser scanning confocal microscope (Zeiss) using the following excitation/emission settings for acquiring fluorescence images: HS-169: ligand 550/599-751 nm; lipofuscin 405/545-615 nm, LL-5: ligand 550/599-751; lipofuscin 405/545-615, and the following excitation wavelengths for spectral recording: LL-1: 535 nm, LL-5: 535 nm, LL-6: 550 nm and LL-7: 535 nm.

Ligand double staining: Sections of frontal cortex (10 μm) from AD patient were fixed, rehydrated and incubated in PBS as described above (ligand staining). The sections were then incubated with a combination of ligands, 300 nM t-HTAA and 300 nM HS-169 or 300 nM p-FTAA and 300 nm LL-5, in PBS for 30 min at RT. The sections were then washed with PBS three times and mounted with Dako mounting medium for fluorescence (Agilent). The mounting medium was allowed to solidify at least overnight before sealing

the cover slips with nail polish. The sections were analysed using an inverted Zeiss LSM 780 laser scanning confocal microscope (Zeiss) using the following settings: t-HTAA/HS-169: excitation at 405 nm and emission between 471–545 nm (t-HTAA); excitation at 550 nm and emission between 609–744 nm (HS-169), p-FTAA/LL-5: excitation at 490 nm and emission between 490–694 nm. Fluorescence lifetime images were acquired using the same confocal microscope system and the data were recorded by a Becker & Hickl Simple-Tau 152 system (SPC-150 TCSPC FLIM module) with the instrument recording software SPCM version 9.42 in the FIFO image mode using 256 time channels (Becker & Hickl GmbH, Berlin, Germany). For all acquisitions, the pinhole was set to 20.2 μm, and for excitation at 405 nm (t-HTAA), a laser diode 405 nm CW/PS with a repetition rate of 50 MHz was utilized. For excitation at 490 nm (p-FTAA and LL-5) or 550 nm (HS-169), a pulsed tuneable In Tune laser with a repetition rate of 40 MHz was used. Data was analysed in SPCImage version 3.9.4 (Becker & Hickl GmbH, Berlin, Germany). As described previously,[31,42] decays were fitted to a bi-exponential decay and the associated lifetimes and weights were used to calculate an intensity average lifetime for plots and comparison.

Conflict of Interest

The authors declare no conflict of interest.

Data Availability Statement

The data that support the findings of this study are available from the corresponding author upon reasonable request.

[1] A. Ross, M. A. Poirier, *Nat. Med.* **2004**, *10*, S10–S17.
[2] F. Chiti, C. M. Dobson, *Annu. Rev. Biochem.* **2006**, *75*, 333–366.
[3] D. Eisenberg, M. Jucker, *Cell.* **2012**, *148*, 1188–203.
[4] M. D. Benson, J. N. Buxbaum, D. S. Eisenberg, G. Merlini, M. J. M. Saraiva, Y. Sekijima, J. D. Sipe, P. Westermark, *Amyloid* **2020**, *27*, 217–222.
[5] H. Bennhold, *Muench. Med. Wochenschr.* **1922**, *44*,1537–1538.
[6] W. E. Klunk, M. L. Debnath, J. W. Pettegrew, *Neurobiol. Aging* **1994**, *15*, 691–698.
[7] S. D. Styren, R. L. Hamilton, G. C. Styren, W. E. Klunk, *J. Histochem. Cytochem.* **2000**, *48*, 1223–1232.
[8] W. E. Klunk, B. J. Bacskai, C. A. Mathis, S. T. Kajdasz, M. E. McLellan, M. P. Frosch, M. L. Debnath, D. P. Holt, Y. Wang, B. T. Hyman, *J. Neuropathol. Exp. Neurol.* **2002**, *61*, 797–805.
[9] A. S. Crystal, B. I. Giasson, A. Crowe, M.-P. Kung, Z.-P. Zhuang, J. Q. Trojanowski, V. M. Lee, *J. Neurochem.* **2003**, *86*, 1359–1368.
[10] P. S. Vassar, C. F. Culling, *Arch. Pathol.* **1959**, *68*, 487–498.
[11] H. Naiki, K. Higuchi, M. Hosokawa, T. Takeda, *Anal. Biochem.* **1989**, *177*, 244–249.

Chemistry–A European Journal

Research Article
doi.org/10.1002/chem.202203568

Chemistry Europe
European Chemical
Societies Publishing

[12] H. Levine 3rd, *Protein Sci.* **1993**, *2*, 404–410.

[13] W. E. Klunk, H. Engler, A. Nordberg, Y. Wang, G. Blomqvist, D. P. Holt, M. Bergström, I. Savitcheva, G. F. Huang, S. Estrada, M. Ausén, M. L. Debnath, J. Barletta, J. C. Price, J. Sandell, B. J. Lopresti, A. Wall, P. Koivisto, G. Antoni, C. A. Mathis, B. Långström, *Ann. Neurol.* **2004**, *55*, 306–319.

[14] M. Groenning, *J. Chem. Biol.* **2010**, *3*, 1–18.

[15] W. E. Klunk, Y. Wang, G.-F. Huang, M. L. Debnath, D. P. Holt, C. A. Mathis, *Life Sci.* **2001**, *69*, 1471–1484.

[16] C. Dyrager, R. P. Vieira, S. Nyström, K. P. R. Nilsson, T. Storr, *New J. Chem.* **2017**, *41*, 1566–1573.

[17] W. Yang, Y. Wong, O. T. W. Ng, L.-P. Bai, D. W. J. Kwong, Y. Ke, Z.-H. Jiang, H.-W. Li, K. K. L. Yung, M. S. Wong, *Angew. Chem. Int. Ed.* **2012**, *51*, 1804–1810.

[18] W. M. Chang, M. Dakanali, C. C. Capule, C. J. Sigurdson, J. Yang, E. A. Theodorakis, *ACS Chem. Neurosci.* **2011**, *2*, 249–255.

[19] K. Cao, M. Farahi, M. Dakanali, W. M. Chang, C. J. Sigurdson, E. A. Theodorakis, J. Yang, *J. Am. Chem. Soc.* **2012**, *134*, 17338–17341.

[20] K. L. Teppang, R. S. Ehrlich, J. Yang, *Methods Enzymol.* **2020**, *639*, 91–114.

[21] M. Hintersteiner, A. Enz, P. Frey, A.-L. Jaton, W. Kinzy, R. Kneuer, U. Neumann, M. Rudin, M. Staufenbiel, M. Stoeckli, K.-H. Wiederhold, H.-U. Gremlich, *Nat. Biotechnol.* **2005**, *23*, 577–583.

[22] E. E. Nesterov, J. Skoch, B. T. Hyman, W. E. Klunk, B. J. Bacskai, T. M. Swager, *Angew. Chem. Int. Ed.* **2005**, *44*, 5452–5456.

[23] N. Okamura, M. Mori, S. Furumoto, T. Yoshikawa, R. Harada, S. Ito, Y. Fujikawa, H. Arai, K. Yanai, Y. Kudo, *J. Alzheimer's Dis.* **2011**, *23*, 37–48.

[24] A. Schmidt, J. Pahnke, *J. Alzheimer's Dis.* **2012**, *30*, 651–664.

[25] M. Cui, M. Ono, H. Watanabe, H. Kimura, B. Liu, H. Saji, *J. Am. Chem. Soc.* **2014**, *136*, 3388–3394.

[26] H. Fu, M. Cui, P. Tu, Z. Pan, B. Liu, *Chem. Commun.* **2014**, *50*, 11875–11878.

[27] A. Åslund, C. J. Sigurdson, T. Klingstedt, S. Grathwohl, T. Bolmont, D. L. Dickstein, E. Glimsdal, S. Prokop, M. Lindgren, P. Konradsson, D. M. Holtzman, P. R. Hof, F. L. Heppner, S. Gandy, M. Jucker, A. Aguzzi, P. Hammarström, K. P. R. Nilsson, *ACS Chem. Biol.* **2009**, *4*, 673–684.

[28] T. Klingstedt, A. Åslund, R. A. Simon, L. B. G. Johansson, J. J. Mason, S. Nyström, P. Hammarström, K. P. R. Nilsson, *Org. Biomol. Chem.* **2011**, *9*, 8356–8370.

[29] T. Klingstedt, H. Shirani, K. O. A. Åslund, N. J. Cairns, C. J. Sigurdson, M. Goedert, K. P. R. Nilsson, *Eur. J. Chem.* **2013**, *19*, 10179–10192.

[30] S. Nyström, K. M. Psonka-Antonczyk, P. G. Ellingsen, L. B. Johansson, N. Reitan, S. Handrick, S. Prokop, F. L. Heppner, B. M. Wegenast-Braun, M. Jucker, M. Lindgren, B. T. Stokke, P. Hammarström, K. P. R. Nilsson, *ACS Chem. Biol.* **2013**, *8*, 1128–1133.

[31] K. Magnusson, R. Simon, D. Sjölander, C. J. Sigurdson, P. Hammarström, K. P. R. Nilsson, *Prion* **2014**, *8*, 319–329.

[32] R. A. Simon, H. Shirani, K. O. A. Åslund, M. Bäck, V. Haroutunian, S. Gandy, K. P. R. Nilsson, *Chem. Eur. J.* **2014**, *20*, 12537–12543.

[33] T. Klingstedt, H. Shirani, J. Mahler, B. M. Wegenast-Braun, S. Nyström, M. Goedert, M. Jucker, K. P. R. Nilsson, *Chem. Eur. J.* **2015**, *21*, 9072–9082.

[34] J. Rasmussen, J. Mahler, N. Beschorner, S. A. Kaeser, L. M. Häsler, F. Baumann, S. Nyström, E. Portelius, T. Lashley, N. C. Fox, D. Sepulveda-Falla, M. Glatzel, A. L. Oblak, B. Ghetti, K. P. R. Nilsson, P. Hammarström, M. Staufenbiel, L. C. Walker, M. Jucker, *Proc. Natl. Acad. Sci. USA* **2017**, *114*, 13018–13023.

[35] J. D. Ulrich, T. K. Ulland, T. E. Mahan, S. Nyström, K. P. R. Nilsson, V. M. Song, Y. Zhou, M. Reinartz, S. Choi, H. Jiang, F. R. Stewart, E. Anderson, Y. Wang, M. Colonna, D. M. Holtzman, *J. Exp. Med.* **2018**, *215*, 1047–1058.

[36] W. Michno, S. Nyström, P. Wehrli, T. Lashley, G. Brinkmalm, L. Guerard, S. Syvänen, D. Sehlin, I. Kaya, D. Brinet, K. P. R. Nilsson, P. Hammarström, K. Blennow, H. Zetterberg, J. Hanrieder, *J. Biol. Chem.* **2019**, *294*, 6719–6732.

[37] D. Sehlin, X. T. Fang, S. R. Meier, M. Jansson, S. Syvänen, *Sci. Rep.* **2017**, *7*, 17254.

[38] G. M. De Waal, L. Engelbrecht, T. Davis, W. J. S. De Villiers, D. B. Kell, E. Pretorius, *Sci. Rep.* **2018**, *8*, 16798.

[39] A. B. Wreden, L. Fernandes, M. Kelley, A. Pereira-Neves, C. S. Moreira, D. R. da Rocha, F. L. Palhano, *ACS Chem. Neurosci.* **2018**, *9*, 2807–2814.

[40] M. Barth, M. Bacioglu, N. Schwarz, R. Novotny, J. Brandes, M. Welzer, S. Mazzitelli, L. M. Häsler, M. Schweighauser, T. V. Wuttke, D. Kronenberg-Versteeg, K. Fog, M. Ambjørn, A. Alik, R. Melki, P. J. Kahle, D. R. Shimshek, H. Koch, M. Jucker, G Tanriöver, *Mol. Neurodegener.* **2021**, *16*, 54.

[41] H. Shirani, M. Linares, C. Sigurdson, M. Lindgren, P. Norman, K. P. R. Nilsson, *Chem. Eur. J.* **2015**, *21*, 15133–15137.

[42] C. Gustafsson, H. Shirani, P. Leira, D. R. Rehn, M. Linares, K. P. R. Nilsson, P. Norman, M. Lindgren, *ChemPhysChem.* **2021**, *22*, 323–335.

[43] L. Lantz, H. Shirani, T. Klingstedt, K. P. R. Nilsson, *Chem. Eur. J.* **2020**, *26*, 7425–7432.

[44] S. N. S. Vasconcelosa, J. S. Reisa, I. M. de Oliveira, M. N. Balfoura, H. A. Stefani, *Tetrahedron* **2019**, *75*, 1865–1959.

[45] S. B. Mogensen, M. K. Taylor, J-W. Lee, *Molecules* **2020**, *25*, 5950.

[46] A. J. J. Lennox, G. C. Lloyd-Jones, *Chem. Soc. Rev.* **2014**, *43*, 412–443.

[47] T. Klingstedt, C. Blechschmidt, A. Nogalska, S. Prokop, B. Häggqvist, O. Danielsson, W. K. Engel, V. Askanas, F. L. Heppner, K. P. R. Nilsson, *ChemBioChem* **2013**, *14*, 607–616.

[48] U. S. Herrmann, A. K. Schütz, H. Shirani, D. Huang, D. Saban, M. Nuvolone, B. Li, B. Ballmer, A. K. Åslund, J. J. Mason, E. Rushing, H. Budka, S. Nyström, P. Hammarström, A. Böckmann, A. Caflisch, B. H. Meier, K. P. R. Nilsson, S. Hornemann, A. Aguzzi, *Sci. Transl. Med.* **2015**, *7*, 299ra123.

[49] A. K. Schütz, S. Hornemann, M. A. Wälti, L. Greuter, C. Tiberi, R. Cadalbert, M. Gantner, R. Riek, P. Hammarström, K. P. R. Nilsson, A. Böckmann, A. Aguzzi, B. H. Meier, *ACS Chem. Neurosci.* **2018**, *9*, 475–481.

[50] C. König, R. Skånberg, I. Hotz, A. Ynnerman, P. Norman, M. Linares, *Chem. Commun.* **2018**, *54*, 3030–3033.

[51] A. K. Schütz, A. Soragni, S. Hornemann, A. Aguzzi, M. Ernst, A. Böckmann, B. H. Meier, *Angew. Chem. Int. Ed. Engl.* **2011**, *50*, 5956–60.

[52] F. Prelli, E. Castaño, G. G. Glenner, B. Frangione, *J. Neurochem.* **1988**, *51*, 648–651.

[53] D. M. A. Mann, T. Iwatsubo, Y. Ihara, N. J. Cairns, P. L. Lantos, N. Bogdanovic, L. Lannfelt, B. Winblad, M. L. C. Maat-Schieman, M. N. Rossor, *Am. J. Pathol.* **1996**, *148*, 1257–1266.

[54] E. Gkanatsiou, E. Portelius, C. E. Toomey, K. Blennow, H. Zetterberg, T. Lashley, G. Brinkmalm, *Neurosci. Lett.* **2019**, *701*, 125–131.

[55] M. A. DeTure, D. W. Dickson, *Mol. Neurodegener.* **2019**, *14*, 32.

[56] C. Condello, T. Lemmin, J. Stöhr, M. Nick, Y. Wu, A. M. Maxwell, J. C. Watts, C. D. Caro, A. Oehler, C. D. Keene, T. D. Bird, S. G. van Duinen, L. Lannfelt, M. Ingelsson, C. Graff, K. Giles, W. F. DeGrado, S. B. Prusiner, *Proc. Natl. Acad. Sci. USA* **2018**, *115*, E782-E791.

[57] A. A. Stepanchuk, P. A. Barber, T. Lashley, J. T. Joseph, P. K. Stys, *Neurobiol. Dis.* **2021**, *161*, 105540.

[58] H. Liu, C. Kim, T. Haldiman, C. J. Sigurdson, S. Nyström, K. P. R. Nilsson, M. L. Cohen, T. Wisniewski, P. Hammarström, J. G. Safar, *J. Biol. Chem.* **2021**, *297*, 101267.

[59] A. W. P. Fitzpatrick, B. Falcon, S. He, A. G. Murzin, G. Murshudov, H. J. Garringer, R. A. Crowther, B. Ghetti, M. Goedert, S. H. W. Scheres, *Nature* **2017**, *547*, 85–190.

[60] B. Falcon, W. Zhang, A. G. Murzin, G. Murshudov, H. J. Garringer, R. Vidal, R. A. Crowther, B. Ghetti, S. H. W. Scheres, M. Goedert, *Nature* **2018**, *561*, 137–140.

[61] B. Falcon, J. Zivanov, W. Zhang, A. G. Murzin, H. J. Garringer, R. Vidal, R. A. Crowther, K. L. Newell, B. Ghetti, M. Goedert, S. H. W. Scheres, *Nature* **2019**, *568*, 420–423.

[62] W. Zhang, A. Tarutani, K. L. Newell, A. G. Murzin, T. Matsubara, B. Falcon, R. Vidal, H. J. Garringer, Y. Shi, T. Ikeuchi, S. Murayama, B. Ghetti, M. Hasegawa, M. Goedert, S. H. W. Scheres, *Nature* **2020**, *580*, 283–287.

[63] Y. Shi, W. Zhang, Y. Yang, A. G. Murzin, B. Falcon, A. Kotecha, M. van Beers, A. Tarutani, F. Kametani, H. J. Garringer, R. Vidal, G. I. Hallinan, T. Lashley, Y. Saito, S. Murayama, M. Yoshida, H. Tanaka, A. Kakita, T. Ikeuchi, A. C. Robinson, D. M. A. Mann, G. G. Kovacs, T. Revesz, B. Ghetti, M. Hasegawa, M. Goedert, S. H. W. Scheres, *Nature* **2021**, *598*, 359–363.

RESEARCH ARTICLE

Multiple colors. A palette of fluorescent donor-acceptor-donor thiophene-based ligands with distinct photo-physical properties was synthesized. Ligands with specific chemical composition displayed selectivity towards distinct protein aggregates in tissue sections with Alzheimer's disease pathology and by applying different combination of ligands, multiplex spectral detection of distinct protein aggregates could be afforded. We foresee that these ligands will aid in fluorescent assignment of disease-associated protein aggregates.
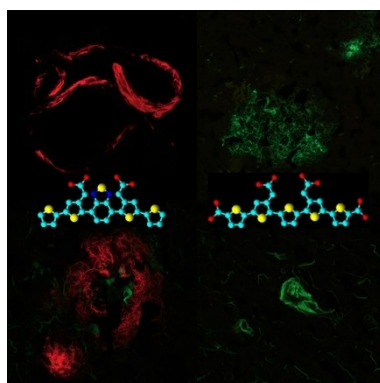
L. Lantz, Dr. H. Shirani, Dr. B. Ghetti, Dr. R. Vidal, Dr. T. Klingstedt, Prof. K. P. R. Nilsson*

1 – 13

Thiophene-Based Ligands for Histological Multiplex Spectral Detection of Distinct Protein Aggregates in Alzheimer's Disease